On bifurcations in a chaotically stirred excitable medium

Shakti N. Menon and Georg A. Gottwald *
School of Mathematics & Statistics, University of Sydney,
New South Wales 2006, Australia

Abstract

We study a one-dimensional filamental model of a chaotically stirred excitable medium. In a numerical simulation we systematically explore its rich bifurcation scenarios involving saddle-nodes, Hopf bifurcations and hysteresis loops. The bifurcations are described in terms of two parameters signifying the excitability of the reacting medium and the strength of the chaotic stirring, respectively. The solution behaviour, in particular at the bifurcation points, is analytically described by means of a nonperturbative variational method. Using this method we reduce the partial differential equations to either algebraic equations for stationary solutions and bifurcations, or to ordinary differential equations in the case of non-stationary solutions and bifurcations. We present numerical simulations corroborating our analytical results.

PACS numbers: 47.54.-r, 47.51.+a, 05.45.-a
Keywords: reaction-diffusion systems; excitable media; chaotic stirring

*corresponding author: gottwald@maths.usyd.edu.au

1 Introduction

Excitable media are abundant in nature, with many examples in biology and chemistry. Examples of excitable media in biological systems include action potential propagation along axons in neural tissue [20], action potential propagation in cardiac tissue [31, 8], cAMP waves in slime moulds [43], calcium waves on the surface of fertilized eggs [26] and plankton dynamics [46]. Examples from chemistry include CO-oxidation on platinum [21] and the Belousov-Zhabotinsky reaction [42, 22]. In addition to biological and chemical contexts excitable media occur in a number of physical systems such as elastic excitable media [5], semiconductor lasers with optical feedback [13] and shock-driven star formation in spiral galaxies [27, 41].

The abundance of excitable media in biological systems is linked to two main characteristics. First, excitable media exhibit threshold behaviour. In zero-dimensional geometry perturbations below a certain threshold immediately decay back to the rest state, whereas super-threshold perturbations grow and decay back to the rest state only after a long excursion. This is crucial for neural and cardiac systems, for example, which would otherwise constantly fire when triggered by small noisy fluctuations rather than by a large stimulus, such as the coordinated stimulation from the sino-atrial node in cardiac dynamics. Second, the decay back to the rest state ensures that the same response of an excitable medium can be expected for a later stimulation, also vital for neural and cardiac function.

In one-dimensional media pulses and wave trains are generic solutions. It is well known that these solutions exhibit a saddle-node bifurcation [34]. When approaching the saddle-node by varying a parameter (usually the excitability), the pulse decreases in width until it becomes too narrow and small to activate the neighbouring medium. This saddle-node bifurcation is responsible for propagation failure in excitable media. In addition, a Hopf bifurcation and a spatial period-doubling bifurcation, which appear close to the saddle-node, were identified as generic bifurcations in excitable media [16].

Active processes such as chemical or biological reactions are often embedded in a fluid flow. This has been well studied in industrial applications such as mixing of reactants within continuously fed or batch reactors [10, 3] and flame filamental structures in combustion systems [40], as well as in several natural contexts such as for the increased depletion of ozone by chlorine filaments [9] and in the development of plankton blooms and the occurrence of plankton patchiness induced by oceanic stirring [47, 1, 28, 29, 30, 19]. A time-dependent and stirring fluid flow can cause interesting effects, which are absent in the unstirred reaction. In particular, the presence of hyperbolic regions of compression and expansion, typical in chaotic flows, results in the evolution of reactants into long thin filaments. This substantially changes the reaction dynamics. The filamentation leads to an increased surface area of the reacting components and associated with this is an increase of the reaction output. If, however, the stirring is too strong the increased thinning of the filaments may lead to a termination of the reaction for the same reasons as in the case of propagation failure in excitable media mentioned above. The corresponding

flow-mediated saddle-node bifurcation has been reported in [36, 24, 23, 32, 7, 33], and in particular for excitable media in [35, 37, 38, 18]. It was observed that the bifurcation scenario of chaotically stirred excitable media was much richer than that of the corresponding unstirred system. However, no systematic analysis of the observed bifurcation scenarios was given.

Our starting point is the question: How are the parameter space and the bifurcations of a chaotically stirred excitable system organized by the two different saddle-nodes corresponding to stirring and to the excitability?

In principle, this problem could be studied by integrating the full two- or three-dimensional reaction–advection–diffusion system. However, this would be computationally very expensive, and an analytical treatment is out of question. In order to describe the behaviour of a stirred reaction-diffusion system one typically resorts to simplified models. In so called filamental or lamellar models [39, 28, 35, 6], the two-dimensional problem of reacting tracers is replaced by a one-dimensional problem of the form

$$\frac{\partial}{\partial t}u_i - \lambda x \frac{\partial}{\partial x}u_i = D_i \frac{\partial^2}{\partial x^2}u_i + \mathcal{F}_i(u_i; k_i) \ , \qquad i = 1, \ldots, n, \tag{1}$$

for n reacting tracers u_i with diffusion coefficients D_i, reaction rates k_i and stirring rate λ. Lamellar models have been employed to study autocatalytic, bistable and excitable media in several physical, chemical and biological contexts [28, 29, 30, 35, 36, 37, 18, 24, 23, 32, 33, 7]. Filamental models such as (1) can be phenomenologically justified by the following picture: The chaotic advection implies hyperbolic regions of stretching and compression as sketched in Fig. 1. Along the stretching direction the concentration is rapidly homogenized leaving no spatial gradients along the filaments. This motivates one to formulate a one-dimensional equation for the direction of compression, i.e. across the filament, only. The compression is parameterized by λ which can be be thought of as the Lagrangian mean strain in the contracting direction, and may be argued to be given by the absolute value of the negative Lyapunov exponent or the (slightly larger) topological entropy. For a different approach to this problem see [44, 45]. The validity of such simplified models has been numerically investigated in [6].

In this paper we aim at providing a systematic numerical and theoretical analysis of the bifurcation scenario of chaotically stirred excitable media. We find supercritical and subcritical Hopf bifurcations and a hysteresis loop besides the well known saddle-node bifurcations associated with propagation failure of excitable media at large Da and at small Da for sufficiently strong stirring. We find that the two saddle-nodes organize the parameter space and the additional bifurcations. Moreover, using a nonperturbative variational approach developed in [15] we analytically investigate the different bifurcations.

In Section 2 we introduce the stirred excitable medium considered in this work. Section 3 provides a thorough numerical investigation of the bifurcation scenario of this model. In Section 4, we review the nonperturbative method to be used to analytically describe the bifurcations and the solutions in terms of equation parameters. This is per-

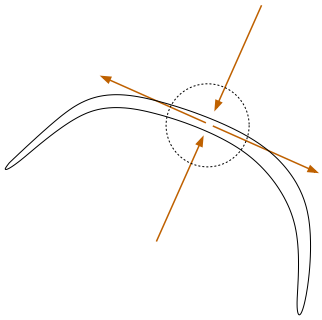

Figure 1: Sketch of a filament in a chaotic flow. An initial blob of reactant (dotted circle) is stretched and compressed by the hyperbolic flow.

formed in Section 5 where we compare the solutions with those of numerical simulations of the full stirred excitable lamellar model. We close with a summary in Section 6.

2 The Model

In this paper we study a filamental model of a chaotically stirred Barkley model [4]

$$\frac{\partial u}{\partial t} = D_u \frac{\partial^2 u}{\partial x^2} + \lambda x \frac{\partial u}{\partial x} + u(1-u)(u-u_s-v) \;, \tag{2}$$

$$\frac{\partial v}{\partial t} = D_v \frac{\partial^2 v}{\partial x^2} + \lambda x \frac{\partial v}{\partial x} + \varepsilon\,(u - a\,v) \;. \tag{3}$$

Here u is the fast activator and v the slow inhibitor. Note that we used a slightly modified formulation of the Barkley model [15]. We expect other one-dimensional excitable media models such as the Fitzhugh-Nagumo model [12] to behave similarly. Here λ denotes the stirring rate, $D_{u,v}$ the respective diffusion constants, u_s the decay rate towards the stable homogeneous rest state $(u,v) = (0,0)$ along the activator directions, and $\varepsilon\, a$ along the inhibitor direction. Note that in the absence of the inhibitor v this equation is a bistable equation. Moreover, the zero-dimensional model including the inhibitor becomes bistable for $a > 1/(1-u_s)$.

In contrast to the unstirred equation, i.e. when $\lambda = 0$, equations (2)–(3) support stationary solutions. This is readily understood by the following phenomenological argument. An initial super-threshold perturbation of the activator at $x = 0$ would develop in the unstirred case into two counter-propagating traveling pulses with a well-defined speed c_0. In the presence of stirring, which is directed towards the origin $x = 0$ with velocity $c_{\rm stir} = -\lambda x$, these waves are stopped when the two velocities are equal. The wave fronts of this stationary solution are then located roughly at $\bar{x} = \pm c_0/\lambda$.

It is customary to rescale the equation and introduce the Damköhler number $Da = k/\lambda$ where k is a typical reaction rate of the process. The Damköhler number measures

the ratio of the reaction rate and the stirring rate. Systems with a small Damköhler number are stirring dominated and those with very high Damköhler numbers are reaction dominated. Scaling $t = t'/\lambda$ and $x = x' D_u/\sqrt{\lambda}$ we write, omitting the primes,

$$\frac{\partial u}{\partial t} = \frac{\partial^2 u}{\partial x^2} + x\frac{\partial u}{\partial x} + Da\, u(1-u)(u-u_s-v)\,, \tag{4}$$

$$\frac{\partial v}{\partial t} = \delta\frac{\partial^2 v}{\partial x^2} + x\frac{\partial v}{\partial x} + Da\,\varepsilon\,(u - a\,v)\,, \tag{5}$$

where $\delta = D_v/D_u$. We will be looking for solutions which are symmetric around $x = 0$ and vanish at $x \to \infty$.

In the following we assume $\delta \ll 1$. This case describes chaotically stirred excitable systems where the activator diffuses at a much faster rate than the inhibitor. A physical realization of this condition may be a chaotically stirred chemical excitable medium such as a stirred Belousov-Zhabotinsky reaction [42, 22] in which the inhibitor is fixed to starch or a gel-like medium. The case $\delta = 0$ is the classic situation in cardiac dynamics. Here the inhibitor consists of (relatively) immobile ion channels. Constant advecting velocities for excitable media in the context of cardiac dynamics is well known for spiral wave drift when subjected to periodic wave trains [25, 11, 48, 14]. An imposed chaotic advecting velocity may be introduced in an analogous way to model the effect of spatially and temporarily random excitations. The source of such random excitations could be either local incoherent stimuli or the cumulative effect of spiral wave chaos.

The steady state solutions ($\partial/\partial t = 0$) of the system (4)-(5) are

$$\frac{d^2 u}{dx^2} + x\frac{du}{dx} + Da\, u(1-u)(u-u_s-v) = 0, \tag{6}$$

$$\delta\frac{d^2 v}{dx^2} + x\frac{dv}{dx} + Da\,\varepsilon\,(u - a\,v) = 0. \tag{7}$$

The equation for the inhibitor is linear and can be solved for given u. In the limiting case $\delta = 0$, the inhibitor $v(x)$ can be explicitly calculated for a given activator $u(x)$ as

$$v(x) = -\frac{2\alpha}{a} x^{2\alpha} \int_{-\infty}^{x} \zeta^{-1-2\alpha} u(\zeta) d\zeta, \tag{8}$$

with $\alpha = Da\,\varepsilon\, a/2$. Note that v inherits the boundary conditions of u.

2.1 Asymptotic solution for small Da

For decreasing values of Da the solution becomes increasingly dominated by stirring until we reach a critical value Da_c where the compression is too strong and below which no non-trivial steady-state solution exists. Below Da_c all initial conditions decay to zero. We now describe the form of the solution close to this stirring induced saddle-node. For small Da we expand u and v as

$$u(x,t) = u_0(x,t) + \mathcal{O}(Da^2) \qquad \text{and} \qquad v(x,t) = v_0(x,t) + \mathcal{O}(Da^2)\,.$$

In this limit the system (4) is solved at leading order by

$$u_0(x,t) = f_0(t)\exp(-w^2(t)x^2)\ ,$$

with $f_0(t) \to 0$ and $w(t) \to 1/\sqrt{2}$ for $t \to \infty$. The temporal decay of the amplitude $f_0(t)$ captures the behaviour for $Da < Da_c$. This is analogous to the bistable case described in [7]. In Fig. 2 we show the solution of u and of v, which is slaved via (5) to u, for small Da confirming the bell-shaped character of the solution close to the saddle-node. Note that although Da_c is an $\mathcal{O}(1)$ quantity the full solution is still well approximated by the shape given by the asymptotic solution. We will use this result later in our variational nonperturbative approach in Section 4 and in Section 5.

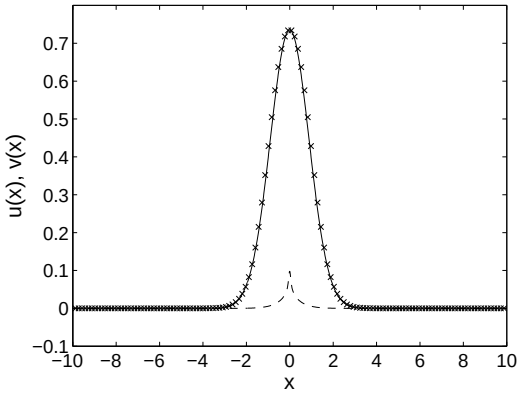

Figure 2: Steady state solution of (6)-(7) for the activator $u(x)$ (stars) and the inhibitor $v(x)$ (dashed line) at $Da = 6.5$ close to the critical stirring induced saddle-node Da_c. The continuous line is a Gaussian fit to the data. Other parameters are $u_s = 0.1$, $a = 0$ and $\varepsilon = 0.005$.

2.2 Asymptotic solution for large Da

For large Damköhler numbers we expect the system to behave like the unstirred system. Indeed, by zooming into the the small spatial scale $\xi = \sqrt{Da}x$ we may transform (4)–(5) into the unstirred steady-state equations up to $\mathcal{O}(1/Da)$. The location of the steady-state solution is given, as discussed above, by the balance of the outward directed diffusion and the inward directed compression of the flow. This location is located at some $\nu = \sqrt{Da}\bar{w}$ where $\bar{w}$ is some $\mathcal{O}(1)$ quantity. Hence we scale

$$\xi = \sqrt{Da}(x - \sqrt{Da}\bar{w})\ , \tag{9}$$

to obtain

$$\frac{\partial^2 u}{\partial \xi^2} + \bar{w}\frac{\partial u}{\partial \xi} + u(1-u)(u-u_s-v) \;=\; \mathcal{O}(Da^{-1})\ , \tag{10}$$

$$\delta\frac{\partial^2 v}{\partial \xi^2} + \bar{w}\frac{\partial v}{\partial \xi} + \varepsilon\,(u - a\,v) \;=\; \mathcal{O}(Da^{-1})\ . \tag{11}$$

This is the equation for an unstirred Barkley model in the frame of reference moving with a constant speed $c_0 = \bar{w}$. This is accordance with the phenomenological argument presented above that the spatial location of the steady-state solution is given as the balance of the stirring velocity and the velocity c_0 of the unstirred system.

We observe numerically that the profile of the steady-state solution is close to the one of the unstirred case when shifted and spatially scaled according to (9), see Fig. 3.

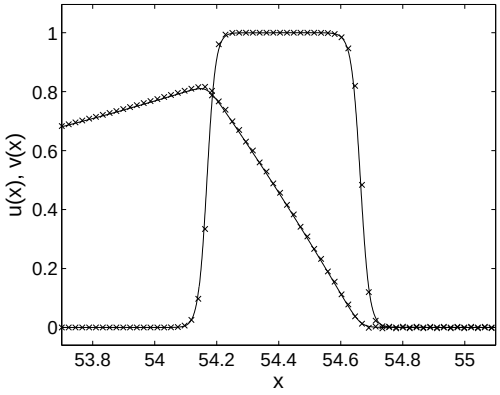

Figure 3: Steady state solution of the plateau like activator $u(x)$ and the inhibitor $v(x)$ at $Da = 10,000$, $u_s = 0.1$, $a = 0.22$ and $\varepsilon = 0.01$. The crosses denote the solution of the stirred system (4)–(5). The continuous lines depict the solution of the rescaled unstirred system (10)–(11) at the same parameters, confirming the asymptotic limit for large Da.

3 Numerical simulations of the model equation

In this Section we present results from a numerical investigation of the full system (4)–(5). This system exhibits two saddle-nodes, one induced by increasing the excitability ε over a threshold value ε_c for fixed (large enough) Damköhler number, and one induced by the stirring when decreasing Da below a critical value Da_c for a given (small enough) ε. We therefore study the solution behaviour in the Da-ε parameter space to investigate the effect of stirring and excitability. We will see that interesting bifurcations and solution behaviour arises due to the way these two saddle-nodes connect.

We numerically integrate the system (4)–(5) using a semi-implicit Crank-Nicolson scheme where the nonlinearities are solved by an Adams-Bashforth method. The case of a non-diffusive inhibitor $\delta = 0$ is numerically problematic as it implies a singular derivative of the inhibitor at $x = 0$ when the activator u is a bell-shaped function which is the case near the saddle-node bifurcations (cf. (8)). We therefore choose for our numerical simulations a value of $\delta = 0.001$ to avoid numerical instabilities. We have numerically checked that the solution of the small diffusion limit converges to the case $\delta = 0$ by observing that the difference of the solutions scales as δ.

A comprehensive picture of the solution behaviour in the Da-ε parameter space is given in Fig. 4.

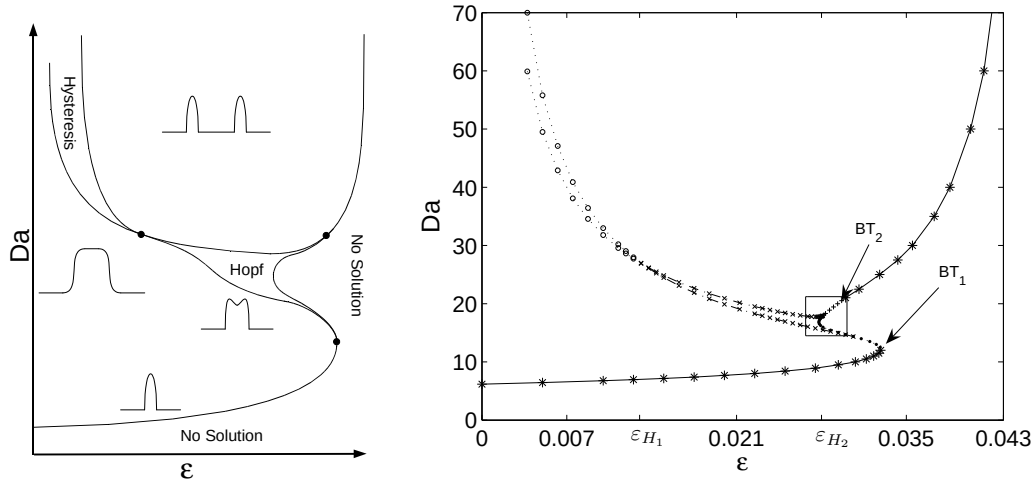

(a) (b)

Figure 4: Solution behaviour in Da-ε parameter space for the system (4)-(5). (a) Sketch of the solution behaviour. The filled circles represent some of the high codimension points observed in the system. (b) Results of numerical simulations for $a = 0$. The lower and upper stability branches, which are represented by stars, correspond to the saddle-node bifurcations arising from the stirring and propagation failure respectively. The branch of the stirring induced saddle-node is found to end at around $\varepsilon \approx 0.0329$, while the branch of the saddle-node due to propagation failure asymptotes for $Da \to \infty$ to $\varepsilon \approx 0.044$, which is the critical value for unstirred media. A region of stable oscillatory solutions arising from a Hopf bifurcation (represented by crosses) is located between two high codimension points at $\varepsilon_{H_1} = 0.013$ and $\varepsilon_{H_2} \approx 0.028$. In the region $\varepsilon \in (0, \varepsilon_{H_1})$, two branches, represented by circles, enclose a region of hysteresis where two stable stationary solutions coexist. These two branches connect with the two branches of the Hopf bifurcation at $\varepsilon = \varepsilon_{H_1}$. These Hopf branches connect with the lower and upper saddle-node branches in a Bogdanov-Takens bifurcation at $\varepsilon \approx 0.0329$ and $\varepsilon \approx 0.03$ respectively (marked as BT). The box around ε_{H_2} encloses a region with a number of different solution behaviours, which is seen in more detail in Fig. 11.

In the following we will explore the different dynamical regions depicted in Fig. 4. We fix $u_s = 0.1$ and $a = 0$, however the dynamical scenarios we report are robust with respect to changes in these parameters.

We first discuss the case of large Damköhler numbers. In Section 2.2 we showed that the solution of the stirred system behaves asymptotically like the unstirred system. Far away from the saddle-node, the solution for large Damköhler numbers consists of two well separated pulses symmetric around $x = 0$ as seen in Fig. 5. The profile of these large

Damköhler number solutions is the same as in the scaled unstirred system (see Fig. 3).

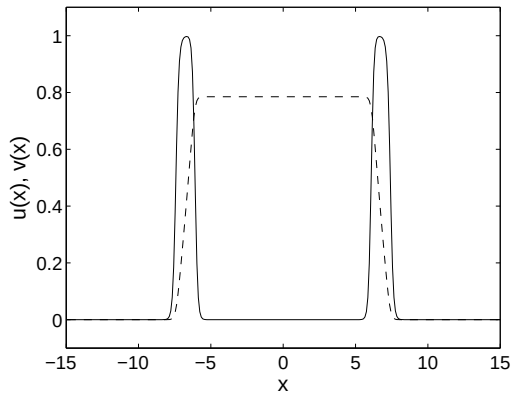

Figure 5: Activator $u(x)$ (continuous line) and inhibitor $v(x)$ (dashed line) for $a = 0$, $\varepsilon = 0.02$ at $Da = 200$ obtained from the numerical simulation of (4)-(5).

Since the system (4)-(5) behaves for large Damköhler numbers like the unstirred system, in this regime we expect the generic saddle-node bifurcation of excitable media [16]. For each sufficiently large Damköhler number there exists a critical value $\varepsilon_c(Da)$ such that there are no solutions for $\varepsilon > \varepsilon_c(Da)$. Close to this saddle-node each of the two pulses assumes a bell-shaped character [15]. As we approach $\varepsilon_c(Da)$, the separation between the two pulses decreases. The stability boundary corresponding to this saddle-node is shown in Fig. 4. This saddle-node has been extensively studied [49, 34, 15].

Besides the saddle-node for large Damköhler numbers which is inherent to excitable media, an additional saddle-node occurs which is induced by the compressive effects of the stirring. For each $\varepsilon \in (0, 0.0329)$ there exists a critical Damköhler number $Da_c(\varepsilon)$ such that there are no solutions for $Da < Da_c(\varepsilon)$. The stability boundary is shown in Fig. 4. For small values of ε near this saddle-node bifurcation, the solution profile of $u(x)$ is approximately bell-shaped for both stable and unstable solutions. Upon increasing Da the solution shape of the stable solution becomes plateau-like, while the unstable solution will remain bell-shaped (as seen in Fig. 6a). For larger values of ε, the stable and unstable solutions near the saddle-node split into a pair of slightly separated pulses due to the increased influence of the inhibitor $v(x)$. On increasing Da the profiles for both solutions will split further into a pair of slightly separated pulses (as seen in Fig. 6b). This had previously been observed in the case of equal diffusion coefficients for activator and inhibitor [18].

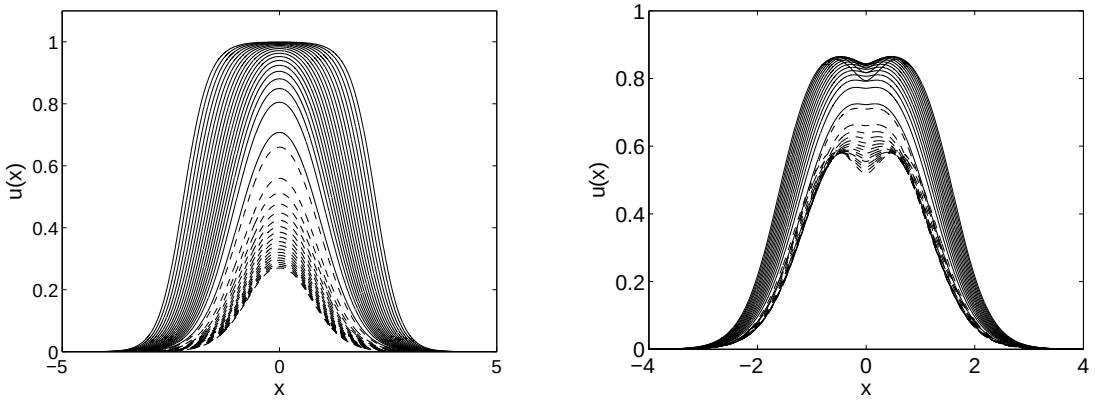

(a) (b)

Figure 6: The numerical solutions of $u(x)$ for the steady system (6)-(7) for $a = 0$. The stable solutions (solid lines) and unstable solutions (dashed lines) are both shown for logarithmically spaced values of Da. (a) For $\varepsilon = 0.005$, we take 20 values between $Da = 25$ and $Da = 6.44$ ($\approx Da_c$). (b) For $\varepsilon = 0.03$, we take 15 values between $Da = 14$ and $Da = 9.65$ ($\approx Da_c$).

At moderate to large Damköhler numbers we observe for $\varepsilon \in (0, 0.013)$ a hysteresis loop between two critical values of the Damköhler number, which we denote as $Da_{hys_1}(\varepsilon)$ and $Da_{hys_2}(\varepsilon)$ for the lower and upper values respectively. In this region, represented by circles in Fig. 4b, we find that two distinct stable solutions coexist as shown in Fig. 7a. For $Da \lesssim Da_{hys_1}(\varepsilon)$ the solution consists of one single pulse centred at $x = 0$, while for $Da \gtrsim Da_{hys_2}(\varepsilon)$ the solution consists of two separated pulses. The hysteresis manifests itself as follows: Increasing the Damköhler number from $Da < Da_{hys_1}(\varepsilon)$ the solution remains plateau-like until $Da = Da_{hys_2}(\varepsilon)$ above which the solution rapidly changes to a pair of two separated plateaus. Conversely, decreasing the Damköhler number from $Da > Da_{hys_2}(\varepsilon)$ a pair of separated plateaus is observed until $Da = Da_{hys_1}(\varepsilon)$ at which point we find a rapid transition to the single plateau-like solution. We find that both Da_{hys_1} and Da_{hys_2} are asymptotic to $\varepsilon = 0$, and the difference between Da_{hys_1} and Da_{hys_2} increases as we approach $\varepsilon = 0$.

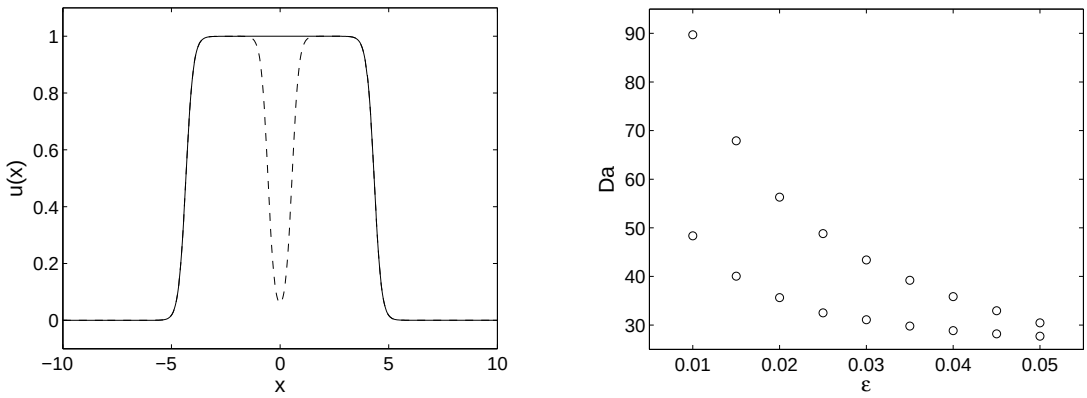

(a) (b)

Figure 7: (a) Profiles of the two stable solutions of $u(x)$ observed for $a = 0$, $\varepsilon = 0.0375$ and $Da = 65$ obtained from the numerical solution of (4)-(5). The plateau-like solution (represented by a solid line) is obtained using an initial condition of a solution profile below Da_{hys_1}, while the two separated pulses (represented by a dotted line) are obtained with an initial condition of a solution profile above Da_{hys_2}. (b) The two branches of the hysteresis loop for $a = 1$ in Da-ε parameter space.

This existence of a hysteresis loop is robust against changes of the parameters a and u_s. In fact the hysteresis becomes increasingly pronounced as we approach the bistable limit $a = 1/(1 - u_s)$. Comparing the extent of the hysteresis loop in Fig. 4b and Fig. 7b, the difference between $Da_{hys_1}(\varepsilon)$ and $Da_{hys_2}(\varepsilon)$ for $a = 1$ (see Fig. 7b) much larger than for corresponding values of ε for $a = 0$ (see Fig. 4b). The existence of a hysteresis region in a stirred excitable medium can be explained by the simultaneous limit of $Da \to \infty$ in which the system (4)-(5) becomes an unstirred excitable medium, and of $\varepsilon \to 0$ in which the system becomes bistable. The two solutions within the hysteresis loop approach the limiting solution types of each limit, with the single plateau-like solution being associated with the bistable equation and the two separated solutions being associated with the unstirred excitable medium. (Note that we use "bistable" here in two ways. The bistable region refers to bistable behaviour within the stirred excitable medium, whereas the limit $\varepsilon = 0$ or $a = 1/(1-u_s)$ refer to the equations becoming the so called "bistable equation".)

For moderate Damköhler numbers and $\varepsilon \in (0.013, 0.03)$ we observe stable oscillations. For fixed ε the oscillations occur for a finite range of Damköhler numbers between Da_{H_1} and $Da_{H_2} > Da_{H_1}$. Unlike in unstirred excitable media these oscillations arise through a supercritical Hopf bifurcation [16]. The Hopf bifurcation is mediated through the interaction of the inhibitors of the two pulses across $x = 0$. Close to the Hopf bifurcation the solution consists of two closely neighbouring pulses (see Fig. 8).

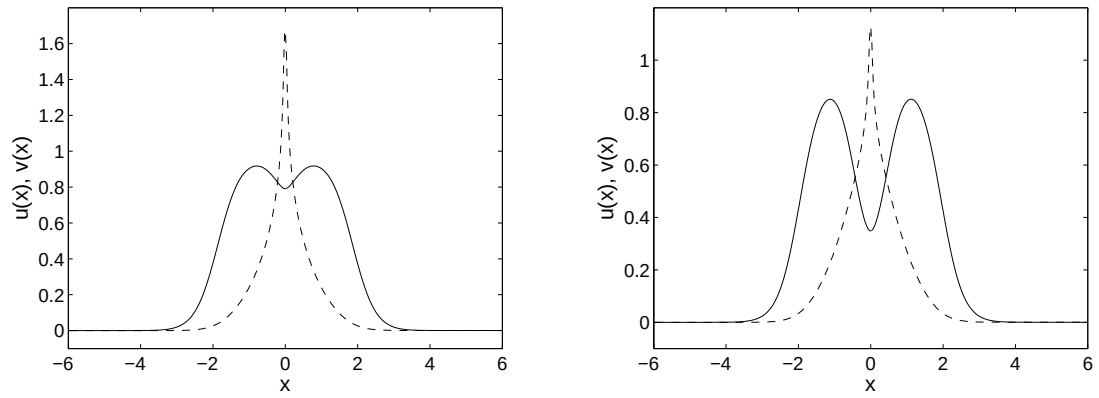

(a) (b)

Figure 8: (a) The activator $u(x)$ and inhibitor $v(x)$ close the Hopf bifurcations. Parameters are $a = 0$, $\varepsilon = 0.025$. (a) $Da = 16.9 \lesssim Da_{H_1}$. (b) $Da = 18.5 \gtrsim Da_{H_2}$.

At $\varepsilon = 0.013$ the region of stable oscillations connects with the hysteresis loop in a higher codimension bifurcation. At larger values of ε the Hopf bifurcation connects in two Bogdanov-Takens bifurcations with the saddle-nodes described above (see Fig. 11).

In Fig. 9 we show the time periodic amplitudes for different values of ε and Da. We see clearly that when approaching the high-codimension point at $\varepsilon = 0.013$, where the Hopf bifurcation coalesces with the hysteresis loop, the period of the oscillations diverge indicating a homoclinic bifurcation. In Fig. 10a, the profiles of the solution of $u(x)$ and of $v(x)$ at the crest and trough of the oscillations in Fig. 9a are shown. We see that the outer sides of the solution $u(x)$ are virtually unaffected during the oscillations, while the region near the origin at $x = 0$ changes significantly, indicating the weak interaction with the tails of the inhibitor.

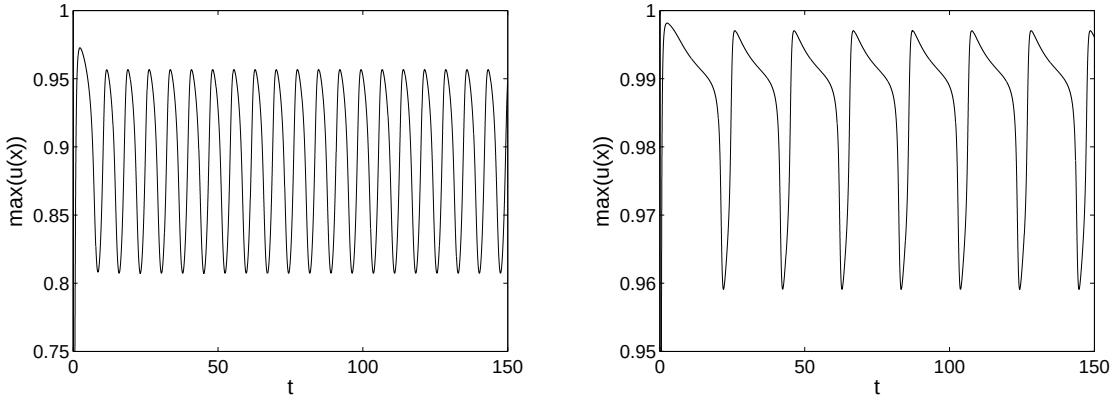

(a) (b)

Figure 9: Plots of the maximal amplitude of $u(x)$ as a function of time, obtained from the numerical solution of (4)-(5), for parameters $a = 0$ and (a) $\varepsilon = 0.025$, $Da = 17.5$, and (b) $\varepsilon = 0.015$, $Da = 24.5$.

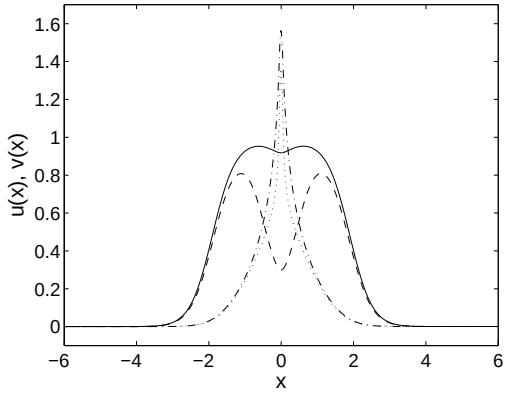

Figure 10: Snapshots of the activator $u(x)$ and the inhibitor $v(x)$, obtained from the numerical solution of (4)-(5) for $a = 0$, $\varepsilon = 0.025$ and $Da = 17.5$. The solid/dashed-dotted line shows $u(x)/v(x)$ at the crest of the oscillation of the solution represented in Fig. 9a, while the dashed/dotted line shows $u(x)/v(x)$ at the trough of the oscillation.

In the region where the Hopf bifurcation coalesces with the saddle-node bifurcations we observe a complex unfolding of bifurcations, as illustrated in Fig. 11. In this region we observe two Bogdanov-Takens points where the two branches of the Hopf bifurcation meet the two saddle-node branches. We find that a number of different solution behaviours are possible in this region, and here we present some of the main observed behaviours. We note that this list is non-exhaustive, and we expect that this system exhibits even more regions of different solution behaviour near the high-codimension points.

We first note that near $\varepsilon \approx 0.028$ a small region exists where stable oscillatory solutions coexist with stable stationary solutions. This region of bistability is labelled C in Fig. 11 and is characterised by a hysteresis loop. If we start with the profile of the stable stationary solution obtained at a value of Da just above this region (i.e. from region A in Fig. 11), then we obtain stable stationary solutions within region C. If, on the other hand, we start with the profile of a snapshot of the stable oscillatory solution obtained at a value of Da just below this region (i.e. from region D in Fig. 11), then we obtain stable oscillatory solutions within the region C. So in fact, region C exhibits bistability where for every value of Da and ε, the stable solution behaviour is either stationary or oscillatory.

Next to this region of bistability, we find a region labelled B in Fig. 11 in which the observed solution behaviour again depends strongly on the initial condition. If we start with the profile of the stable stationary solution obtained at a value of Da just above this region (i.e. from region A), stable stationary solutions are observed in this region. If we start from the bistability region C, then the observed behaviour depends on the nature of the solution type as described above. Specifically, if the initial condition is that of the stable stationary solution in C, the solution behaviour in B is also stable and stationary. On the other hand, if we choose an initial condition given by the profile of a stable oscillatory solution in C, then we find that the solution dies out to $u = 0$ as we cross the boundary between the two regions. The time periods of the oscillations in region C rapidly increase close to the boundary with B which is is indicative of a homoclinic bifurcation.

We further observe that region B has a stability boundary with region E where no solutions are observed. As we move from B to E we observe that the solution dies out to $u = 0$ via a subcritical Hopf bifurcation. This is reminiscent of the generic bifurcation behaviour in unstirred excitable systems for weakly interacting pulses [17]. As we move from region D to E the time period of the oscillations increases rapidly (not shown here), and the solution goes to zero. This is again indicative of a homoclinic bifurcation. The two homoclinic bifurcations, i.e between D and E and between C and B, join up at the high codimension point $\varepsilon \approx 0.028$. The homoclinic bifurcation branches between C and B coalesces with the subcritical Hopf bifurcation as well as the saddle-node branch of the propagation failure at $\varepsilon \approx 0.03$. We also find that the homoclinic bifurcation branch between D and E coalesces with the lower branch of the supercritical Hopf bifurcations, Da_{H_1}, and the saddle-node branch due to stirring at a Bogdanov-Takens point $\varepsilon \approx 0.0329$.

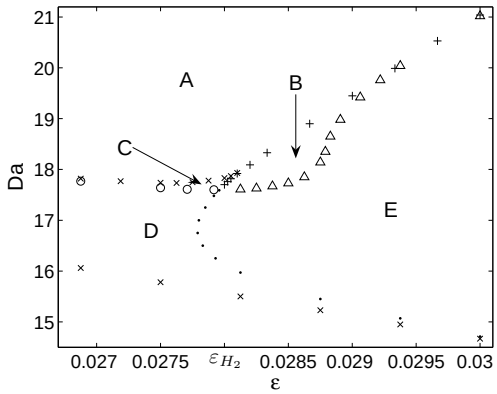

Figure 11: Close up of the region $\varepsilon \in (0.0265, 0.031)$ of the $Da - \varepsilon$ parameter space shown in Fig. 4. Region A contains stable stationary solutions, region D contains stable oscillatory solutions and region E contains no solutions (these three regions have been depicted in Fig. 4). The branches of a supercritical Hopf bifurcation are represented by crosses. In region B we have a strong dependence on initial conditions. At the stability boundary between regions B and E (represented by triangles), we observe a subcritical Hopf bifurcation. In region C, we find that stable stationary solutions coexist with stable oscillatory solutions. At the boundary between regions C and D (represented by circles) we observe a second supercritical Hopf bifurcation. The oscillatory solutions in D and C flatten out to $u = 0$ in a homoclinic bifurcation represented by plus signs and dots respectively. A high codimension point at $\varepsilon_{H_2} \approx 0.028$ is marked.

4 Nonperturbative variational method

In [15] a nonperturbative variational method was developed which was particularly useful in describing the solution behaviour and bifurcations in cases when asymptotic techniques failed. This is the case, for example, near the saddle-node when the solution assumes a bell-shape and is not separable into a flat outer solution and a steep narrow inner solu-

tion. The method in [15] restricts the "shape" of the solution to a specified test function, and then determines the parameters of this test function in a projection procedure which minimizes the error made by the restriction. The method has been used in excitable, autocatalytic, bistable and combustions systems [32, 7, 33].

In particular, we restrict the solutions to the form

$$u(x,t) = U(x,p_i(t)) , \quad i = 1,\ldots,n , \tag{12}$$
$$v(x,t) = V(x,q_j(t)) , \quad j = 1,\ldots,m , \tag{13}$$

where the test function U is parameterized by parameters $p_i(t)$, and V by $q_j(t)$. Note that for the case of steady-state solutions we may calculate $v(x)$ as a function of $u(x)$ using (7) or (8) (for $\delta = 0$). Hence to study stationary bifurcations it is sufficient to specify U and p_i. In the following we still keep V and q_j explicit to illustrate the method.

Once we restrict the solutions of the system (4)–(5) to a particular solution space of the test functions spanned by (12) and (13), we look for those parameters p_i and q_j which optimize this approximation. This is achieved by requiring the error to be orthogonal to the tangent space of the restricted test function solution space, which is spanned by $\partial U/\partial p_i$ and $\partial V/\partial q_j$ This condition assures that the error lies in the orthogonal complement of the function space spanned by the prescribed test functions. Our conditions determining the free parameters p_i and q_j are therefore

$$\langle -U_t + U_{xx} + xU_x + Da\,U(1-U)(U-u_s-V) \mid \partial U/\partial p_i \rangle_x = 0 , \tag{14}$$
$$\langle -V_t + \delta V_{xx} + xV_x + Da\,\varepsilon\,(U - a\,V) \mid \partial V/\partial q_j \rangle_x = 0 , \tag{15}$$

where the brackets indicate integration over the whole x domain. Using

$$\frac{\partial U}{\partial t} = \sum_{i=1}^{n} \frac{\partial U}{\partial p_i}\dot{p}_i \qquad \text{and} \qquad \frac{\partial V}{\partial t} = \sum_{j=1}^{m} \frac{\partial V}{\partial q_j}\dot{q}_j ,$$

we obtain a system of $m+n$ coupled ordinary differential equations for the parameters p_i and q_j. For stationary bifurcations we may ignore the time-dependence of the parameters and end up with a set of algebraic equations instead. Note that if U is specified, V can be calculated explicitly in the stationary case as a function of U by solving the ordinary differential equation (7) with only (14) as the variational condition.

We will employ two different choices of test functions. Close to the saddle-node bifurcations where the activator u assumes a bell-shaped profile (see Fig. 2) we may choose a Gaussian function

$$U(\eta,t) = f_0(t)\exp(-\eta^2) \qquad \text{with} \qquad \eta = w(t)x , \tag{16}$$

where the parameters are $\{p_i\} = \{f_0, w\}$. In this case (7) can be solved analytically and V can be given explicitly (cf. Section 5.3). The approach is not restricted to a particular

test function. For bell-shaped functions one may equally take sech- or sech^2-functions [7]. A more general test function which is able to describe a variety of different shapes such as single or twin plateau-like solutions is given by

$$\begin{aligned} U(\eta,t) = \frac{g_0}{2} \big(&\tanh\left(\eta - \omega(\mu-\nu)\right) + \tanh\left(\eta + \omega(\mu+\nu)\right) \\ &- \tanh\left(\eta - \omega(\mu+\nu)\right) - \tanh\left(\eta + \omega(\mu-\nu)\right) \big)\,, \end{aligned} \tag{17}$$

where the parameters are $\{p_i\} = \{g_0, \omega, \nu, \mu\}$ and $\eta = \omega x$, where ω measures again the steepness of the solution. This test function is particularly well suited to study chaotically stirred excitable media. It is able to capture all solution profiles we discovered in Section 3. In particular, it allows us to describe the time-varying solution profile of the solution in the region near the Hopf bifurcation with two interacting pulses. The range of solution types of (17) is illustrated in Fig. 12. In the case when (17) describes two separated single pulses, the maximum of the pulses is a distance μ apart from the center $x = 0$ and has half-width ν. Note that the maximal amplitude is not given by g_0 but rather by $U(x = \mu, t)$. In this case V has to be numerically evaluated by solving the ordinary differential equation (7). Note that one could restrict the analysis just to the positive domain $x \geq 0$. However, we will consider here the whole domain since it poses no further computational effort.

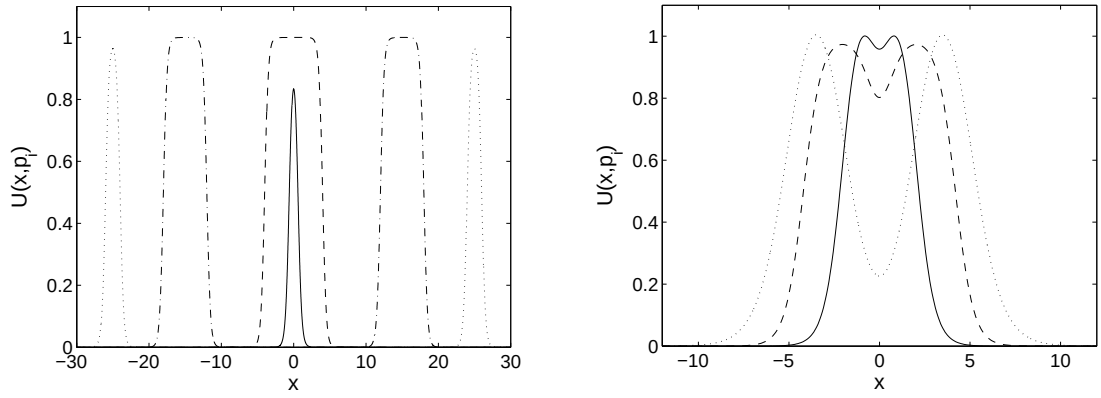

(a) (b)

Figure 12: Different profiles obtained using the test function (17) for different values of the parameters $p_i = \{g_0, \omega, \nu, \mu\}$. The solution describes: (a) Pulse-like shape for $p_i = \{1, 2, 0.3, 0.3\}$ (solid line). Plateau-like shape for $p_i = \{1, 2, 2, 2\}$ (dashed line). "Twin-plateau" shape for $p_i = \{1, 2, 3, 15\}$ (dashed-dotted line). "Twin-pulse" shape for $p_i = \{1, 2, 1, 25\}$ (dotted line). (b) Examples of closely neighbouring pulses which appear near the Hopf bifurcations; solid line: $p_i = \{1.25, 1, 0.9, 1.1\}$, dashed line: $p_i = \{1, 1, 2, 2.2\}$, dotted line: $p_i = \{1.4, 0.6, 1.5, 3.5\}$.

For completeness we provide here the basis functions of the tangent space correspond-

ing to the test function (17)

$$\frac{\partial U}{\partial g_0} = \frac{1}{g_0} U, \quad \frac{\partial U}{\partial \nu} = \frac{g_0\,\omega}{2}\left(s_1 + s_2 + s_3 + s_4\right), \quad \frac{\partial U}{\partial \mu} = \frac{g_0\,\omega}{2}\left(-s_1 + s_2 + s_3 - s_4\right),$$
$$\frac{\partial U}{\partial \omega} = \frac{g_0}{2\omega}\left((\eta - \omega(\mu-\nu))s_1 - (\eta - \omega(\mu+\nu))s_2 + (\eta + \omega(\mu+\nu))s_3 - (\eta + \omega(\mu-\nu))s_4\right),$$

where $s_1 = \mathrm{sech}^2(\eta - \omega(\mu - \nu))$, $s_2 = \mathrm{sech}^2(\eta - \omega(\mu + \nu))$, $s_3 = \mathrm{sech}^2(\eta + \omega(\mu + \nu))$ and $s_4 = \mathrm{sech}^2(\eta + \omega(\mu - \nu))$.

In the following Section we will use this variational approach to study the solutions and the bifurcations we discovered in Section 3.

5 Results of the nonperturbative variational approach

In this section we compare the results obtained using the nonperturbative method with those of the numerical simulations of the full system (4)–(5) (and its steady-state formulation (6)–(7)), as presented in Section 3. We will use the nonperturbative method to study the solution behaviour for large Damköhler numbers, the saddle-node associated with propagation failure at large Da, the stirring-induced saddle-node at small Da and the hysteresis loop at intermediate values of the Damköhler number. The Hopf bifurcation is analyzed by a time-dependent version of the variational approach.

5.1 Solutions for large Damköhler numbers

For large enough values of Da the solution of (4)-(5) consists of two stationary pulses, symmetric around $x = 0$, as illustrated in Fig. 5. Far away from the saddle-node reported in Section 3, the pulses take the form of a plateau-type solution for small values of ε, while for larger values of ε approaching $\varepsilon_c(Da)$ they become bell-shaped. We perform the nonperturbative approach for a test function of the form (17) which is able to capture both solution types. The nonperturbative method for the test function (17) consists of four algebraic equation consisting of the four projections (14) for the parameters $\{g_0, \omega, \mu, \nu\}$. We show in Fig. 13 a comparison with numerical results of the full system (4)-(5). Fig. 13a reveals that the amplitude approaches for $Da \to \infty$ the constant value $f_0 = 0.9989$ corresponding to the amplitude of the unstirred system. (Note that the maximal amplitude for the test function (17) is not given by f_0 but rather by $U(x = \mu)$). The distance from the origin $x = 0$ is roughly measured by μ which scales with $\sqrt{Da}$, as illustrated in Fig. 13b, consistent with the asymptotic theory of Section 2.2.

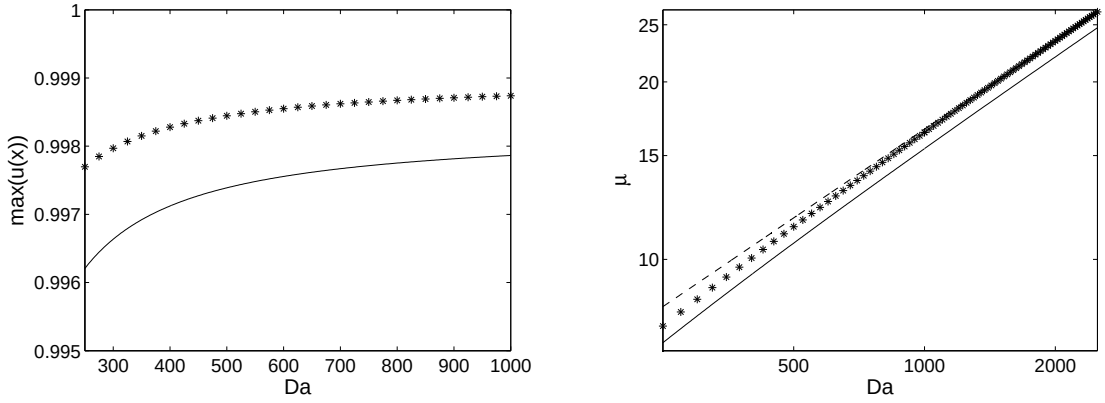

(a) (b)

Figure 13: Comparison of the numerical solution (stars) of (4)-(5) with the corresponding values of the nonperturbative method for a test function (17) (continuous line) for $\varepsilon = 0.02$ and $a = 0$. (a) Maximal amplitude of the pulses. (b) Logarithmic plot of the distance of the pulses from $x = 0$. A reference line with slope 1/2 is given.

5.2 Saddle-node bifurcation at large Damköhler numbers

At large Damköhler numbers there exists a critical $\varepsilon_c(Da)$ above which propagation failure sets in. This saddle-node is inherent to excitable media. At the saddle-node the activator is bell-shaped as shown in Fig. 2. The asymptotic analysis in Section 2.2 showed that the system (4)-(5) is equivalent to the unstirred system (10)-(11). This allows us to use the results of [15] for excitable unstirred media directly. The projection (14) with a bell-shaped test function such as (16) with $\tilde{U} = \exp(-\eta^2)$ can be formulated as [15]

$$Af_0^2 + Bf_0 + C = 0 \,, \tag{18}$$

where

$$\begin{aligned} A &= \tfrac{3}{4}\langle\tilde{U}^4\rangle - \tfrac{5}{6}\langle\tilde{U}^3V\rangle - \tfrac{a\Theta}{3}\langle\eta\tilde{U}^3V\rangle \,, \\ B &= -\tfrac{5}{6}(1+u_s)\langle\tilde{U}^3\rangle + \langle\tilde{U}^2V\rangle + \tfrac{a\Theta}{2}\langle\eta\tilde{U}^2V\rangle \,, \quad C = u_s\langle\tilde{U}^2\rangle \,. \end{aligned} \tag{19}$$

where $\Theta = \varepsilon Da/\mu w$. Here $v(\eta) = f_0 V(\eta)$ and $v(\eta)$ is the solution of (11) which we write in the rescaled version as

$$V_\eta = -\frac{\varepsilon Da}{\mu w}(U - aV) \,.$$

The corresponding inverse width parameters $w_\pm$ for the stable and unstable branch are given by

$$w^2 = \frac{1}{D\langle\tilde{U}_\eta^2\rangle}[f_0^2(-\langle\tilde{U}^4\rangle + \langle\tilde{U}^3V\rangle) + f_0((1+u_s)\langle\tilde{U}^3\rangle - \langle\tilde{U}^2V\rangle) - u_s\langle\tilde{U}^2\rangle] \,. \tag{20}$$

The velocity $\bar{w}$ can now be determined in the standard way by multiplying the equation for the activator u (4) by u_x and integrating over x. We obtain

$$\bar{w} = -\frac{f_0\Theta}{w\langle\tilde{U}_\eta^2\rangle}[\frac{f_0}{3}(\langle\tilde{U}^4\rangle - a\langle\tilde{U}^3V\rangle) - \frac{1}{2}(\langle\tilde{U}^3\rangle - a\langle\tilde{U}^2V\rangle)] \,. \tag{21}$$

Note that $\mu \approx \bar{w}\sqrt{Da}$.

We also perform a nonperturbative analysis using the tanh-based test function (17). This does not allow for an explicit formula but the condition (14) has to be numerically evaluated for the parameters $\{f_0, g_0, \omega, \mu, \nu\}$. In Fig. 14 we show a comparison of the two different test functions comparing with results from a simulation of the full system (4)-(5). The plot shows that for large Da both test functions yield good agreement with the full system. Note in particular that the variational approach produces the quadratic behaviour typical for a saddle-node (see (18)), as illustrated in Fig. 14.

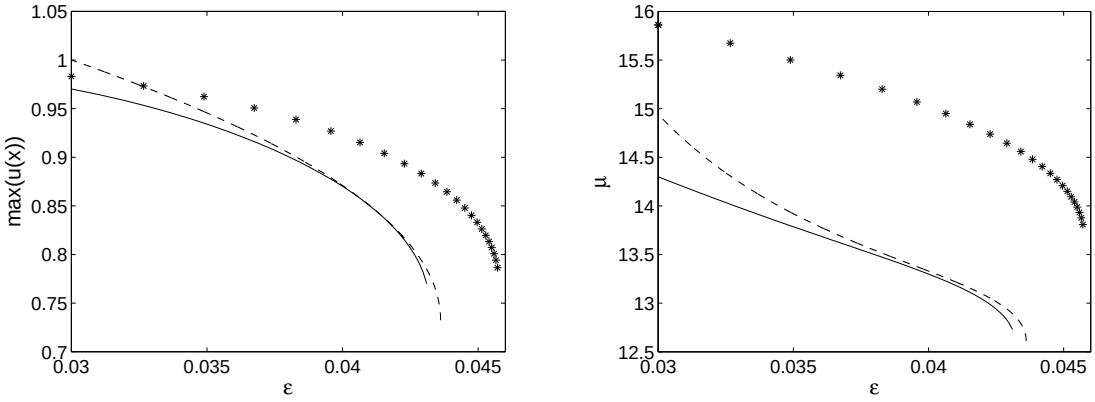

(a) (b)

Figure 14: Comparison of the numerical solution (represented by stars) of (4)-(5) with the corresponding values of the nonperturbative method for $Da = 1000$ and $a = 0$. The analytical formula (18) and (21) for a Gaussian test function (16) is depicted as a dashed line. The results from a numerical evaluation of (14) for a test function (17) is depicted as a solid line. (a) Maximal amplitude of the pulses. (b) Distance of the pulses from $x = 0$.

5.3 Saddle-node bifurcation at small Damköhler numbers

Besides the saddle-node at large Da which is generic for excitable systems there is an additional saddle-node associated with the stirring of the system. For smaller values of the Damköhler number the pulses become too quenched and cannot sustain excitation anymore. Note that small Damköhler numbers does not mean $Da \approx 0$, but refers rather to the range of finite Damköhler numbers below which no solutions exist (see Fig. 4). We will now describe this saddle-node explicitly using our variational nonperturbative method. Guided by our asymptotic analysis in Section 2.1 and numerical observation (see Fig. 2), we use a Gaussian test function ansatz (16)

$$U(\eta) = f_0 \exp(-\eta^2) \qquad \text{with} \qquad \eta = wx \ .$$

The inhibitor $v(x)$ can then be given explicitly via (8) as

$$V(\eta) = \frac{f_0\,\alpha}{a}\,\eta^{2\alpha}\Gamma(-\alpha, \eta^2), \tag{22}$$

where again we set $\alpha = Da\,\varepsilon\,a/2$, and where $\Gamma(-\alpha,\eta^2)$ is the incomplete Gamma function

$$\Gamma\left(\alpha,x\right)=\int_x^\infty \varsigma^{\alpha-1}e^{-\varsigma}d\varsigma\,. \tag{23}$$

As discussed in Section 4, we project onto the tangent space of the restricted solution subspace spanned by

$$\frac{\partial U}{\partial f_0}=\frac{1}{f_0}U \qquad \text{and} \qquad \frac{\partial U}{\partial w}=\frac{1}{w}\eta U'\,,$$

and require

$$\begin{aligned}\langle w^2\,U_{\eta\eta}+\eta\,U_\eta+Da\,U(1-U)(U-u_s-V)\;\mid\;U\rangle_\eta &= 0\,, &(24)\\ \langle w^2\,U_{\eta\eta}+\eta\,U_\eta+Da\,U(1-U)(U-u_s-V)\;\mid\;\eta U_\eta\rangle_\eta &= 0, &(25)\end{aligned}$$

where the integration is performed over the whole η domain, and $V(\eta)$ is given by (22). These are two algebraic equations for the two unknown parameters f_0 and w. This system can be solved analytically (see Appendix) to obtain the following quadratic equation for the amplitude f_0

$$Af_0^2+Bf_0+C=0\,,$$

which is solved by

$$f_0=\frac{-B\pm\sqrt{B^2-4AC}}{2A}\,, \tag{26}$$

and an algebraic equation for the inverse pulse width w

$$w^2=Da\left[f_0^2\left(\sqrt{\frac{2}{\pi}}K(3)-\frac{1}{\sqrt{2}}\right)-f_0\left(\sqrt{\frac{2}{\pi}}K(2)-(1-u_s)\sqrt{\frac{2}{3}}\right)-\left(u_s+\frac{1}{2\,Da}\right)\right]\,, \tag{27}$$

where

$$\begin{aligned}A=&\frac{9a+8\alpha}{24a}\sqrt{\pi}-\frac{5+4\alpha}{6}K(3),\\ B=&-\frac{5a\,(1+u_s)+6\alpha}{6a}\sqrt{\frac{\pi}{3}}+(\alpha+1)\,K(2),\\ C=&\sqrt{\frac{\pi}{2}}\left(u_s+\frac{1}{Da}\right)\,.\end{aligned} \tag{28}$$

The function $K(n)$ is given by

$$K(n)=\frac{\alpha}{a}\Gamma\left(-\alpha\right)\Gamma\left(\alpha+\frac{1}{2}\right)n^{-\frac{1}{2}-\alpha}+\frac{1}{a}\sqrt{\frac{\pi}{n}}\,{}_2F_1\left(\left\{\frac{1}{2},-\alpha\right\};\{1-\alpha\};-\frac{1}{n}\right)\,. \tag{29}$$

The limit $a\to 0$ allows for the following simplification

$$K(n)=Da\,\varepsilon\sqrt{\frac{\pi}{n}}\,\mathrm{arcsinh}\big(\sqrt{n}\big)\,. \tag{30}$$

The quadratic equation (26) for the amplitude f_0 yields the stable and unstable solutions. For $B^2 - 4AC = 0$ these solutions coalesce and then subsequently vanish in a saddle-node bifurcation. The condition $B^2 - 4AC = 0$ determines the bifurcation point Da_c. Once the amplitude f_0 is determined we may calculate the inverse width w using (27).

The expressions for the amplitude f_0 simplify in certain limits. In the Appendix we shall describe in detail how the bistable case of [32, 7] is recovered in the limit $\varepsilon \to 0$ when the inhibitor is constant and the system (4)-(5) is no longer excitable, but bistable. In the limit of $Da \to \infty$ we find that in accordance with the asymptotic calculation of Section 2.2 we recover the results for the unstirred Barkley model found in [15] and used in Section 5.2.

We observe that the variational test function method captures the actual dynamics of the full system (4)-(5) well. In Fig. 15, we compare the analytical results for the amplitude (26) with those of a numerical simulation of (6)-(7). We also perform the nonperturbative approach using the tanh-based test function (17). The comparison is clearly better for the tanh-based test function than for the Gaussian test function for larger values of ε. Although the solution close to the saddle-node bifurcation is well approximated by a Gaussian test function as evidenced by Fig. 6, the solution for larger values of ε develops rapidly into two separate interacting pulses with increasing Damköhler number, as seen in Fig. 6b. This explains the better performance of the more versatile tanh-based test function when compared to the simpler Gaussian test function (16). Fig. 15 also reveals that the unstable solution is well approximated by a Gaussian, typical for these systems [7].

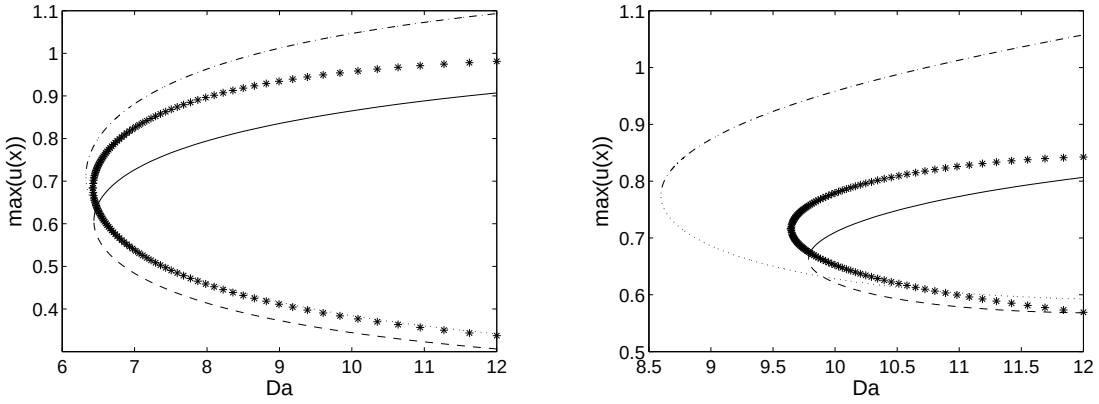

(a) (b)

Figure 15: Comparison of the amplitude f_0 of the stable and unstable solution as a function of the Damköhler number Da at $a = 0$. Shown are results from a simulation of (6)-(7) (stars), the analytical formula (26) for a Gaussian test function (16) (dashed-dotted line for stable, dotted line for unstable branch), and the nonperturbative approach using the tanh-based test function (17) (continuous line for stable, dashed line for unstable branch). (a) $\varepsilon = 0.005$. (b) $\varepsilon = 0.03$.

In Fig. 16 we show a comparison between the activator $u(x)$ as calculated from numerically integrating the full equations (6)-(7) and the variational test function approach for a Gaussian with parameters f_0 and w calculated via (26) and (27).

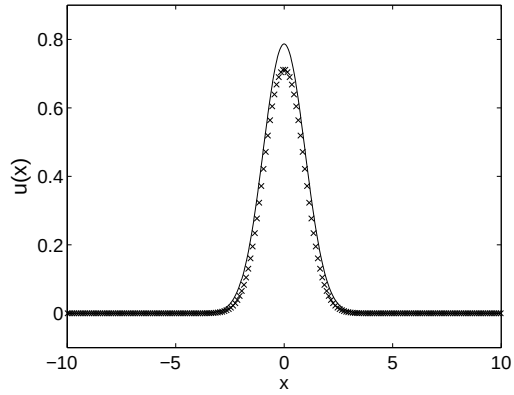

Figure 16: The activator $u(x)$ obtained from the numerical solution of the system (6)-(7) (stars) at $Da = 6.45$, $a = 0$ and $\varepsilon = 0.005$ superimposed with the Gaussian test function (continuous line) with parameters f_0 and w calculated using (26) and (27).

As for the parameters f_0 and w of the Gaussian test function, the critical Damköhler numbers Da_c, as calculated from the criterion $B^2 - 4AC = 0$ for a Gaussian test function, matches up well for small values of ε but rather poorly for larger values as seen in Fig. 17. Again this is due to the stronger deviation of the solution from a Gaussian shape for larger values of ε. The results of the nonperturbative method for the tanh-based test function show excellent agreement with the results from the full system (6)-(7).

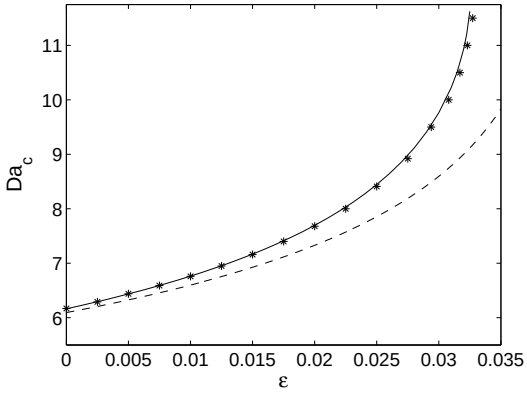

Figure 17: Comparison of the critical value of the Damköhler number at the saddle-node Da_c calculated using the critical condition $B^2 - 4AC = 0$ of the Gaussian test function method (dashed line) with the value as calculated from a numerical simulation of the full system (6)-(7) (stars) for $a = 0$. The continuous line shows results from the test function approach using the tanh-based test function (17).

5.4 Hysteresis Loop

For small values of ε and sufficiently large Damköhler numbers we observe a region of bistability. The bistability is linked to the different asymptotic solutions at the respective limits of $\varepsilon \to 0$ and $Da \to \infty$. In the limit $\varepsilon \to 0$ the system (4)-(5) is not excitable anymore but bistable and the solution consists of a single plateau-like solution. In the limit $Da \to \infty$ the stirred system behaves like an unstirred excitable medium and has two well separated pulses symmetrically arranged around the origin at $x = 0$. In the simultaneous limit $\varepsilon \to 0$ and $Da \to \infty$ both solution types coexist as shown in Fig. 18. The region of bistability is more pronounced for larger values of a approaching the bistable limit $a = 1/(1 - u_s)$. We therefore take $a = 1$ in the following.

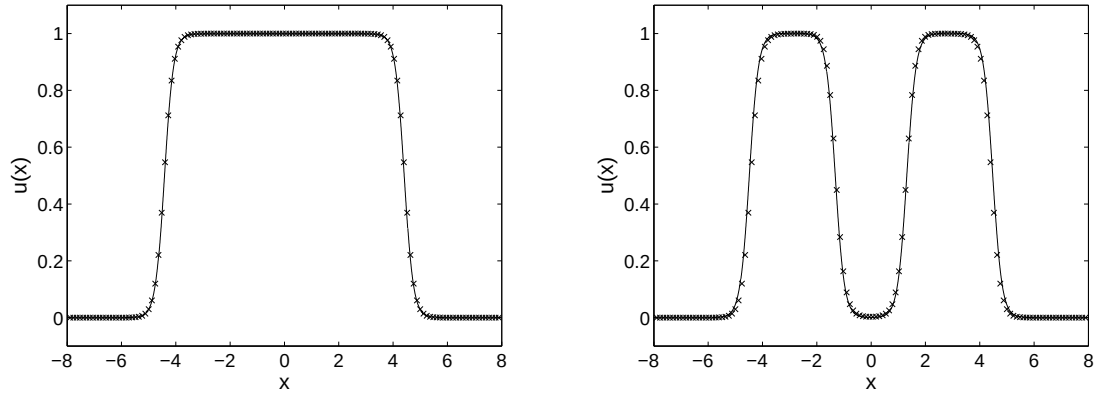

(a) (b)

Figure 18: Stationary solutions $u(x)$ in the bistable region at $Da = 70$, $a = 1$ and $\varepsilon = 0.01$. The solution obtained by numerical integration of the full system (4)-(5) is shown as points. The continuous line shows the result of our test function approach using the tanh-based test function (17) with excellent agreement. (a) The plateau-like solution at this value of Da. (b) The twin plateau-like solution at this value of Da.

The bistable region is characterized by a hysteresis loop which is illustrated in Fig. 19, and the solution of (4)-(5) in the bistable region depends on the initial condition. In Fig. 19 we show the hysteresis loop and provide a comparison of our nonperturbative test function approach using a tanh-based test function (17) with results from the simulation of the full system (4)-(5). The test function approach clearly captures both solution types exhibiting bistability. The nonperturbative method approximates the solution well and is able to detect the bifurcation at Da_{hys_1}. The upper bifurcation point Da_{hys_2} is largely overestimated by the test function approach as can be clearly seen from Fig. 19. This can be linked to the near-degeneracy of the stable and unstable branches at large Damköhler numbers. In the test function approach the unstable solution of the twin plateau-solution coincides for large Da with the stable branch of the single plateau solution. The kink of the unstable branch of the single plateau solution as seen in Fig. 19 stems from the functional change of the unstable solution at this point from a single pulse solution to a twin pulse solution.

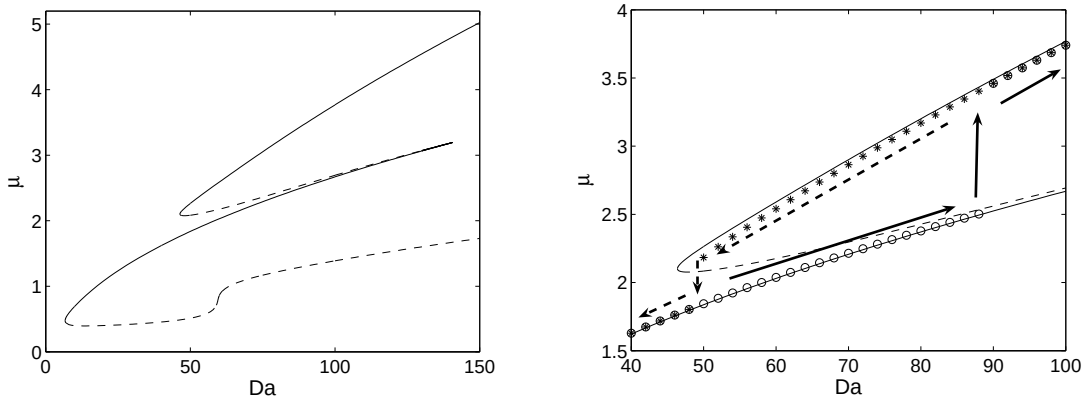

(a) (b)

Figure 19: Pulse location μ as a function of Da for $\varepsilon = 0.01$ and $a = 1$ illustrating the hysteresis loop. (a) Result of the nonperturbative approach by evaluating (14) for a test function (17). Stable branches are depicted by continuous lines, unstable branches by dashed line. (b) Results of the numerical simulation of (4)-(5) with results from the nonperturbative approach. The numerical results obtained when starting with a plateau-like solution and increasing the value of Da are represented by circles, while the results obtained when starting with a twin plateau-like solution and decreasing Da are represented by stars. The arrows indicate the hysteresis loop. Note the near-degenerate behaviour of the lower stable and unstable branches.

5.5 The Hopf Bifurcation

In this section we use a time-dependent version of the test function approach to describe the Hopf bifurcation at moderate values of the Damköhler number. We choose the tanh-based test function (17), and now take time dependent parameters $\{g_0(t), \omega(t), \mu(t), \nu(t)\}$. In the time-independent case we prescribed only the functional form of the activator U, and subsequently could determine the inhibitor V which is slaved to the activator using the exact equation (7). In the time-dependent case we cannot simply determine V as a function of U by solving the ordinary differential equation (7). However, observation of numerical simulations suggests the following simple ansatz for the inhibitor in the time-dependent case

$$V(x,t) = h_0(t) \exp(-|\zeta|) \quad \text{with} \quad \zeta = \kappa(t)\, x \; . \tag{31}$$

The associated basis functions of the tangent space needed for the projection are then

$$\frac{\partial V}{\partial h_0} = \frac{V}{h_0}, \quad \frac{\partial V}{\partial \kappa} = \frac{\zeta\, V_\zeta}{\kappa} \; . \tag{32}$$

As described in Section 4 the projection of the equations onto the tangent space yields a system of 4+2 first order ordinary differential equations for the parameters $\{g_0(t), \omega(t), \mu(t), \nu(t)\}$

and $\{h_0(t), \kappa(t)\}$, (14) and (15), which we write here as

$$\sum_{j=1}^{4} \left\langle \dot{p}_j \frac{\partial U}{\partial p_j} \mid \frac{\partial U}{\partial p_i} \right\rangle_\eta = \left\langle \omega^2 U_{\eta\eta} + \eta U_\eta + Da\, U(1-U)(U - u_s - V) \mid \frac{\partial U}{\partial p_i} \right\rangle_\eta , \quad (33)$$

$$\sum_{j=1}^{2} \left\langle \dot{q}_j \frac{\partial V}{\partial q_j} \mid \frac{\partial V}{\partial q_i} \right\rangle_\zeta = \left\langle \delta\kappa^2 V_{\zeta\zeta} + \zeta V_\zeta + Da\, \varepsilon\, (U - a\, V) \mid \frac{\partial V}{\partial q_i} \right\rangle_\zeta , \quad (34)$$

with $\{p_i(t)\} = \{g_0(t), \omega(t), \mu(t), \nu(t)\}$ and $\{q_i(t)\} = \{h_0(t), \kappa(t)\}$.

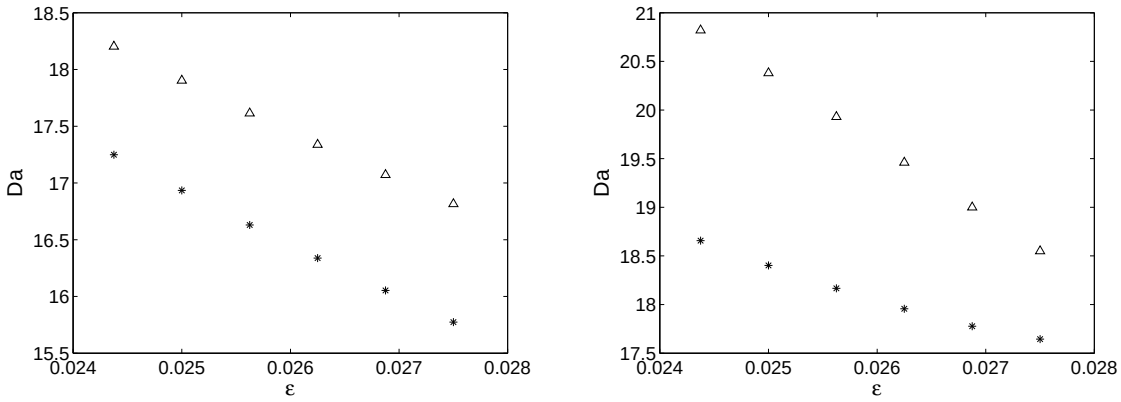

(a) (b)

Figure 20: Comparison of the critical Damköhler number of the Hopf bifurcation as a function of ε at $a = 0$, calculated via the nonperturbative method (represented by triangles) with the corresponding values obtained from a numerical solution of the system (4)-(5) (represented by stars). (a) Lower branch, Da_{H_1}. (b) Upper branch, Da_{H_2}.

As we see in Fig. 20, the values of Da_{H_1} and Da_{H_2} as calculated via the nonperturbative method match up fairly well with the numerically obtained values of these critical points. In Fig. 21 we show the time period T of the oscillations. A comparison of the values obtained by a numerical simulation of the full partial differential equations (4)-(5) and the reduced ordinary differential equations (33) and (34), obtained from the nonperturbative approach, show good qualitative agreement.

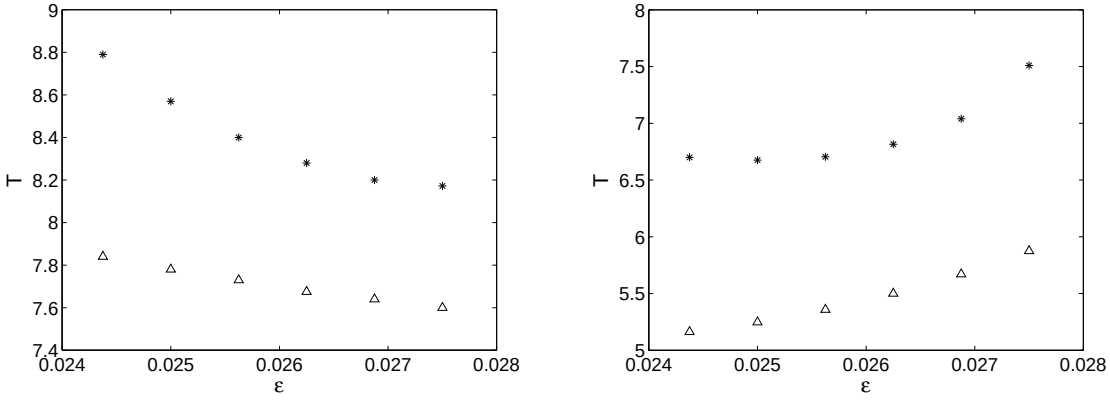

(a) (b)

Figure 21: Comparison of the time period T of the oscillations at the critical Damköhler number of the Hopf bifurcation as a function of ε at $a = 0$ calculated via the nonperturbative method (represented by triangles) with the corresponding values obtained from a numerical solution of the system (4)-(5) (represented by stars). (a) Time period at the lower branch, Da_{H_1}. (b) Time period at the upper branch, Da_{H_2}.

6 Summary

We studied the effect of stirring on an excitable system using a one-dimensional filament model. In particular, we examined a system where the diffusion coefficient of the activator is much larger than that of the inhibitor. We found that the bifurcation scenarios are organized around two saddle-node bifurcations separating the Da-ε parameter space into a part with no solutions and a part with various steady and unsteady pulse solutions. We identified one of the saddle-nodes as the generic saddle-node for excitable media, and another saddle-node as the generic saddle-node for chaotically stirred reaction-diffusion systems. We also found a region of bistable behaviour and an associated hysteresis loop. Within this bistable region we find the two solution types characteristic for the limit $Da \to \infty$ and $\varepsilon \to 0$. Connecting to the bistable region in a homoclinic bifurcation we find two Hopf branches. Unlike in unstirred excitable media, the Hopf bifurcation is supercritical. Close to higher codimension bifurcations, where the Hopf branches collide with the saddle-node bifurcations, we found complex unfoldings including bistability between stable stationary and stable oscillatory solutions.

We applied a nonperturbative method developed in [15] to describe the bifurcation behaviour. This approach restricts the solution space to specified test functions which are parameterized by a set of variables whose dynamics is used to optimize the fit. This approach is similar to the method of collective coordinates. This nonperturbative approach allowed us to reduce the steady-state equations (6)-(7) to a set of algebraic equations for the parameters of the test function, and the partial differential equations (4)-(5) to a set of ordinary differential equations. We showed that the nonperturbative approach captures the bifurcation scenarios and the solution behaviour well, and hence allows for

an effective reduced description of the full system.

A Calculation of the parameters of a Gaussian test function using the nonperturbative method

Here we describe in detail the calculations involved in finding the explicit expressions of the parameters of a Gaussian test function (16) with the nonperturbative method near the saddle-node bifurcation at Da_c for $\delta = 0$. We then simplify the expressions for the limit $\varepsilon \to 0$ to the bistable case already studied in [32, 7], and for the limit $Da \to \infty$ to the case of unstirred Barkley model as studied in [15].

We restate the conditions for the minimization of the error, (24) and (25),

$$\begin{aligned} \langle w^2\, U_{\eta\eta} + \eta\, U_\eta + Da\, U(1-U)(U-u_s-V) \mid U \rangle_\eta &= 0\,, \qquad (35) \\ \langle w^2\, U_{\eta\eta} + \eta\, U_\eta + Da\, U(1-U)(U-u_s-V) \mid \eta U_\eta \rangle_\eta &= 0\,. \qquad (36) \end{aligned}$$

For a test function which vanishes at $x \to \pm\infty$ we can simplify the following integrals using partial integration, for $n > 0$,

$$\langle \eta U_{\eta\eta} U_\eta \rangle = -\frac{1}{2}\langle U_\eta^2 \rangle\,, \qquad \langle \eta U_\eta U^n \rangle = -\frac{1}{n+1}\langle U^{n+1} \rangle\,.$$

Using the equation for the inhibitor for the limiting case $\delta = 0$

$$\eta V_\eta = -Da\,\varepsilon\,(U - a\,V)\,,$$

we may simplify the expression

$$\begin{aligned} \langle \eta U^{n-1} U_\eta V \rangle &= -\frac{1}{n}(\langle \eta U^n V_\eta \rangle + \langle U^n V \rangle) \\ &= -\frac{1}{n}\langle U^n V \rangle + \frac{1}{n} Da\,\varepsilon(\langle U^{n+1} \rangle - a\langle U^n V \rangle)\,. \end{aligned}$$

The conditions (35)–(36) can now be combined to give

$$\begin{aligned} \frac{9a+8\alpha}{12a}\langle U^4 \rangle - \frac{5+4\alpha}{6}\langle U^3 V \rangle - \frac{5a\,(1+u_s)+6\alpha}{6a}\langle U^3 \rangle \\ + (1+\alpha)\,\langle U^2 V \rangle + \left(u_s + \frac{1}{Da}\right)\langle U^2 \rangle = 0\,, \end{aligned} \qquad (37)$$

where we have taken $\alpha = Da\,\varepsilon a/2$.

The integrals of the type $\langle U^n\, V \rangle$ can be evaluated by considering the solution of $V(\eta)$ for the limiting value $\delta = 0$. When U is given by a Gaussian test function, i.e. $U(\eta) = f_0 \exp(-\eta^2)$, we find that V is given by (22), which we recall

$$V(\eta) = \frac{f_0\,\alpha}{a}\,\eta^{2\alpha}\Gamma(-\alpha, \eta^2)\,.$$

Writing the incomplete Gamma function in terms of an infinite sum [2] (eqn. (6.5.29)), we get the following expression

$$V(\eta) = \frac{f_0\,\alpha}{a}\,\eta^{2\alpha}\left(\Gamma(-\alpha) + \eta^{-2\alpha}\sum_{j=0}^{\infty}\frac{(-1)^j\,\eta^{2j}}{j!\,(\alpha-j)}\right).$$

The integral $\langle U^n V\rangle$ can now be explicitly written as

$$\begin{aligned}\langle U^n\,V\rangle =& \frac{f_0\,\alpha}{a}\Gamma(-\alpha)\int_{-\infty}^{\infty}\eta^{2\alpha}U^n(\eta)d\eta \\ &+ \frac{f_0\,\alpha}{a}\int_{-\infty}^{\infty}U^n(\eta)\sum_{j=0}^{\infty}\frac{(-1)^j\,\eta^{2j}}{j!\,(\alpha-j)}d\eta\,.\end{aligned}$$

As U is a Gaussian test function, this simplifies to

$$\begin{aligned}\langle U^n\,V\rangle = \frac{f_0^{n+1}\,\alpha}{a}\Bigg(&\Gamma(-\alpha)\,\Gamma(\alpha+1/2)\,n^{-1/2-\alpha} \\ &+\sum_{j=0}^{\infty}\int_{-\infty}^{\infty}e^{-n\eta^2}\frac{(-1)^j\,\eta^{2j}}{j!\,(\alpha-j)}d\eta\Bigg),\end{aligned} \tag{38}$$

where the order of integration and summation has been reversed for the second integral. The integral over η can be found explicitly, and the summation is found to yield

$$\sum_{j=0}^{\infty}\frac{(-1)^j\,n^{-1/2-j}\Gamma(j+1/2)}{j!\,(\alpha-j)} = \frac{1}{\alpha}\sqrt{\frac{\pi}{n}}\,{}_2F_1\left(\{1/2,-\alpha\};\{1-\alpha\};-\frac{1}{n}\right).$$

Substituting back into (38), we obtain

$$\begin{aligned}\langle U^n V\rangle =& f_0^{n+1}\left[\frac{\alpha}{a}\Gamma(-\alpha)\,\Gamma\left(\alpha+\frac{1}{2}\right)n^{-\frac{1}{2}-\alpha} + \frac{1}{a}\sqrt{\frac{\pi}{n}}\,{}_2F_1\left(\left\{\frac{1}{2},-\alpha\right\};\{1-\alpha\};-\frac{1}{n}\right)\right] \\ =:& f_0^{n+1}K(n)\ .\end{aligned} \tag{39}$$

Moreover, for a Gaussian test function we can evaluate

$$\langle U^n\rangle = \sqrt{\frac{\pi}{n}}f_0^n\,,\qquad \langle\eta^2U_\eta^2\rangle = \frac{3}{4}\langle U^2\rangle\,.$$

Upon substitution into (37) we obtain the quadratic equation (26) for the amplitude f_0, which we evaluate here as

$$\begin{aligned}\left(\frac{9a+8\alpha}{12a}\sqrt{\frac{\pi}{4}} - \frac{5+4\alpha}{6}K(3)\right)f_0^2 - \left(\frac{5a\,(1+u_s)+6\alpha}{6a}\sqrt{\frac{\pi}{3}} + (1+\alpha)\,K(2)\right)f_0 \\ + \left(u_s+\frac{1}{Da}\right)\sqrt{\frac{\pi}{2}} = 0.\end{aligned}$$

The equation for the inverse width w, (27), can now be found by substituting the expression for f_0 and (39) into (35). In the remainder we study several limits for which the expressions can be simplified.

The limit $\mathbf{a \to 0}$. In the limit $a \to 0$ the inhibitor does not decay anymore in time. Setting $a = 0$ in the equation for the inhibitor (A) and choosing $U(\eta) = f_0 \exp(-\eta^2)$, we get

$$V(\eta) = -\frac{f_0 Da\, \varepsilon}{2} \mathrm{Ei}(-\eta^2),$$

where Ei is the exponential integral

$$\mathrm{Ei}(x) = \int_{-\infty}^{x} \frac{e^{\varsigma}}{\varsigma} d\varsigma \,. \tag{40}$$

The integrals of the form $\langle U^n V \rangle$ can be explicitly evaluated to obtain the simplified form for $K(n)$, as in (30),

$$K(n) = Da\, \varepsilon \sqrt{\frac{\pi}{n}}\, \mathrm{arcsinh}\big(\sqrt{n}\big) \,.$$

The limit $\varepsilon \to 0$. In the limit of vanishing ε the excitable system (4)–(5) becomes bistable, since v is not evolving in time anymore. Upon taking the limit in (28) and using $K(n) = 0$ for $\varepsilon = 0$, we obtain

$$A = \frac{3}{4}\,, \quad B = -\frac{5\,(1+u_s)}{3\sqrt{3}}\,, \quad C = \frac{\sqrt{2}\,(Da\, u_s + 1)}{Da}\,,$$

which corresponds to the result obtained for the bistable system [32, 7].

The limit $\mathbf{Da \to \infty}$. From our asymptotic considerations in Section 2.2 we expect that the limit $Da \to \infty$ recovers the results found in [15] for unstirred excitable media moving in a frame of reference with speed $c_0 = \mu/\sqrt{Da}$, namely (18)–(21). We first show that in the limit $Da \to \infty$ the inhibitor $v(\eta)$ is the same for the stirred and the unstirred system. The equation for the inhibitor in the stirred flow is

$$\eta v_\eta = -\theta(u - av) \,, \tag{41}$$

with $\theta = \varepsilon Da$, the solution of which we now show is asymptotic to the appropriately scaled unstirred equation (11) which we write in rescaled variables as

$$\tilde{v}_\eta = -\Theta(u - a\tilde{v}) \,, \tag{42}$$

with $\Theta = \theta/(\mu w)$, where we used $\eta = wx$ and $\mu = \sqrt{Da}\bar{w}$. The solution of (42) is readily found by variation of constants and reads

$$\tilde{v}(\eta) = -\Theta e^{a\Theta\eta} \int_{-\infty}^{\eta} d\eta'\, e^{-a\Theta\eta'} u(\eta') \,. \tag{43}$$

The solution of the stirred equation (41) is

$$v(\eta) = -\theta\eta^{a\theta}\int_{-\infty}^{\eta} d\eta'\,\eta'^{-a\theta}\frac{1}{\eta'}u(\eta')\ . \tag{44}$$

Using $\lim_{\theta\to\infty}(1+z/\theta)^{\theta} = \exp(z)$ we obtain that for $\theta\to\infty$ (44) converges to

$$\begin{aligned} v(\eta) &= -\theta e^{a\theta\eta}\int_{-\infty}^{\eta} d\eta'\,e^{-a\theta\eta'}\frac{1}{\eta'}u(\eta') \\ &\to -\Theta e^{a\Theta\eta}\int_{-\infty}^{\eta} d\eta'\,e^{-a\Theta\eta'}u(\eta')\ , \end{aligned}$$

where we used that for an activator located at $x=\mu$ with scale w we have $u(wx)/(wx)\to u(wx)/(w\mu)$ for $\mu\to\infty$. Hence in the limit $Da\to\infty$ the inhibitor v of the stirred system (41) converges to the solution $\tilde{v}$ of the unstirred equation (42), i.e. $v=\tilde{v}$ in this limit.

We now show that the algebraic equations (37) for the stirred system (6)-(7) converge to expression (19) for the unstirred equations (10)-(11). We rewrite (37) as

$$Af_0^2 + Bf_0 + C = 0\ ,$$

with

$$\begin{aligned} A &= \frac{3}{4}\langle\tilde{U}^4\rangle - \frac{5}{6}\langle\tilde{U}^3V\rangle + \frac{\theta}{3}(\langle\tilde{U}^4\rangle - a\langle\tilde{U}^3V\rangle)\ , \\ B &= -\frac{5}{6}\left(1+u_s\right)\langle\tilde{U}^3\rangle + \langle\tilde{U}^2V\rangle - \frac{\theta}{2}(\langle\tilde{U}^3\rangle - a\langle\tilde{U}^2V\rangle)\ , \\ C &= \left(u_s + \frac{1}{Da}\right)\langle\tilde{U}^2\rangle\ , \end{aligned}$$

where we used $U=f_0\tilde{U}$. Using (41) we obtain

$$\begin{aligned} A &= \frac{3}{4}\langle\tilde{U}^4\rangle - \frac{5}{6}\langle\tilde{U}^3V\rangle - \frac{1}{3}\langle\eta V_\eta\tilde{U}^3\rangle\ , \\ B &= -\frac{5}{6}\left(1+u_s\right)\langle\tilde{U}^3\rangle + \langle\tilde{U}^2V\rangle + \frac{1}{2}\langle\eta V_\eta\tilde{U}^2\rangle\ , \\ C &= \left(u_s + \frac{1}{Da}\right)\langle\tilde{U}^2\rangle\ . \end{aligned}$$

From the equality of v and $\tilde{v}$ in the limit $Da\to\infty$ we may write

$$V_\eta = -\Theta(U-aV)\ ,$$

and using the evenness of U we obtain in the limit $Da\to\infty$ the expressions for A, B and C in (19).

Acknowledgements We gratefully acknowledge fruitful discussions with Martin Wechselberger. GAG gratefully acknowledges support by the Australian Research Council, DP0452147. SNM was supported by a University of Sydney Postgraduate award.

References

[1] E. R. Abraham, The generation of plankton patchiness by turbulent stirring, Nature **391** (1998) 577–580.

[2] M. Abramowitz and I. A. Stegun, *Handbook of Mathematical Functions with Formulas, Graphs, and Mathematical Tables.* Dover, New York, 1964.

[3] M. A. Allen, J. Brindley, J. Merkin and M. J. Piling, Autocatalysis in a shear flow, Phys. Rev. E **54** (1996) 2140–2142.

[4] D. Barkley, A model for fast computer simulation of waves in excitable media, Physica D **49** (1991) 61–70.

[5] J. H. E. Cartwright, E. Hernández-García and O. Piro, Burridge-Knopoff models as elastic excitable media, Phys. Rev. Lett. **79** (1997) 527–530.

[6] S. M. Cox, Chaotic mixing of a competitive–consecutive reaction, Physica D **199** (2004) 369–386.

[7] S. M. Cox and G. A. Gottwald, A bistable reaction–diffusion system in a stretching flow, Physica D **216** (2006) 307–318.

[8] J. M. Davidenko, A. M. Pertsov, R. Salomonsz, W. Baxter and J. Jalife, Stationary and drifting spiral waves of excitation in isolated cardiac muscle, Nature (London) **335** (1992) 349–351.

[9] S. Edouard, B. Legras, F. Lefèvre and R. Eymard, The effect of small-scale inhomogeneities on ozone depletion in the Arctic, Nature **384** (1996) 444–447.

[10] I. R. Epstein, The consequences of imperfect mixing in autocatalytic chemical and biological systems, Nature **374** (1995) 321–327.

[11] E. A. Ermakova, V. I. Krinsky, A. V. Panfilov and A.M.Pertsov, Interaction between spiral and flat periodic autowaves in an active medium, Biophysics **31** (1986) 318–323.

[12] R. FitzHugh, Impulses and physiological states in theoretical models of nerve membranes, Biophys. J. **1** (1961) 445–466; J. Nagumo, S. Arimoto and S. Yoshizawa, An active pulse transmission line simulating nerve axon, Proc. IRE **50** (1962) 2061–2070.

[13] M. Giudici, C. Green, G. Giacomelli, U. Nespolo and J. R. Tredice, Andronov bifurcation and excitability in semiconductor lasers with optical feedback, Phys. Rev. E **55**, 6 (1997) 6414–6418.

[14] G .A. Gottwald, A. Pumir and V. Krinsky, Spiral wave drift induced by stimulating wave trains, Chaos **11** (2001) 487–494.

[15] G. A. Gottwald and L. Kramer, On propagation failure in one- and two-dimensional excitable media, Chaos **14** (2004) 855–863.

[16] G. A. Gottwald and L. Kramer, A normal form for excitable media, Chaos **16**, 013122 (2006).

[17] G. A. Gottwald, Bifurcation analysis of a normal form for excitable media: Are stable dynamical alternans on a ring possible?, Chaos **18**, 013129 (2008).

[18] E. Hernández-Garcia, C. Lopéz and Z. Neufeld, Filament bifurcations in a one-dimensional model of reacting excitable fluid flow, Physica A **327** (2003) 59–64.

[19] E. Hernández-Garcia and C. Lopéz, Sustained plankton blooms under open chaotic flows, Ecological Complexity **1** (2004) 253–259.

[20] A. L. Hodgkin and A. F. Huxley, A quantitative description of membrane current and its application to conduction and excitation in nerve, J. Physiol. **117**, 4 (1952) 500–544.

[21] S. Jakubith, H. H. Rotermund, W. Engel, A. von Oertzen and G. Ertl, Spatiotemporal concentration patterns in a surface reaction: Propagating and standing waves, rotating spirals, and turbulence, Phys. Rev. Lett. **65** (1990) 3013–3016.

[22] *Chemical Waves and Patterns*, edited by R. Kapral and K. Showalter. Kluwer Academic, Dordrecht, 1993.

[23] I. Z. Kiss, J. H. Merkin, S. K. Scott, P. L. Simon, S. Kalliadasis and Z. Neufeld, The structure of flame filaments in chaotic flows, Physica D **176** (2003) 67–81.

[24] I. Z. Kiss, J. H. Merkin and Z. Neufeld, Combustion initiation and extinction in a 2D chaotic flow, Physica D **183** (2003) 175–189.

[25] V. I. Krinsky and K. I. Agladze, Interaction of rotating waves in an active-chemical medium, Physica D **8** (1983) 50–56.

[26] J. Lechleiter, S. Girard, E. Peralta and D. Clapham, Spiral calcium wave propagation and annihilation in Xenopus laevis ooctyes, Science **252** (1991) 123–126.

[27] B. F. Madore and W. L. Freedman, Computer simulations of the Belousov-Zhabotinsky reaction, Science **222**, 4264 (1983) 615–616.

[28] A. P. Martin, On filament width in oceanic plankton distributions, J. Plank. Res. **22** (2000) 597–602.

[29] A. P. Martin, Phytoplankton patchiness: the role of lateral stirring and mixing, Prog. Oceanograph. **57** (2003) 125–174.

[30] P. McLeod, A. P. Martin and K. J. Richards, Minimum length scale for growth-limited oceanic plankton distributions, Ecological Modelling **158** (2002) 111–120.

[31] A. B. Medvinsky, A. V. Panfilov and A. M. Pertsov, Autowave process characterization in heart tissue, in *Self organization, Autowaves and Structures Far From Equilibrium* edited by V. I. Krinsky. Springer, Berlin, 1984.

[32] S. Menon and G. A. Gottwald, Bifurcations in reaction–diffusion systems in chaotic flows, Phys. Rev. E **71** (2005) 066201.

[33] S. Menon and G. A. Gottwald, Bifurcations of flame filaments in chaotically mixed combustion reactions, Phys. Rev. E **75** (2007) 016209.

[34] E. Meron, Pattern-formation in excitable media, Physics Reports **218**, (1992) 1–66.

[35] Z. Neufeld, Excitable media in a chaotic flow, Phys. Rev. Lett. **87** (2001) 108301.

[36] Z. Neufeld, P. H. Haynes and T. Tél, Chaotic mixing induced transitions in reaction–diffusion systems, Chaos **12** (2002) 426–438.

[37] Z. Neufeld, C. Lopéz, E. Hernández-Garcia and O. Piro, Excitable media in open and closed chaotic flows, Phys. Rev. E **66** (2002) 066208.

[38] Z. Neufeld, P. Haynes, V. Garçon and J. Sudre, Ocean fertilization experiments may initiate a large scale phytoplankton bloom, Geophys. Res. Lett. **29**, (2002) 11.

[39] W. E. Ranz, Applications of a stretched model to mixing, diffusion, and reaction in laminar and turbulent flows, AIChE J. **25** (1979) 41–47.

[40] P. D. Ronney, Some open issues in premixed turbulent combustion, in *Modeling in Combustion Science*, pp. 3–22, Eds. J. Buckmaster and T. Takeno. Springer-Verlag Lecture Notes in Physics, 1994.

[41] L. S. Schulman and P. E. Seiden, Percolation and galaxies, Science **233**, 4762 (1986) 425–431.

[42] S. K. Scott, *Chemical Chaos*, Oxford University Press, New York, 1991.

[43] F. Siegert and C. Weijer, Analysis of optical density wave propagation and cell movement in the cellular slime mould Dictyostelium Discoideum, Physica D **49** (1991) 224–232.

[44] X. Z. Tang and A. H. Boozer, Design criteria of a chemical reactor based on a chaotic flow, Chaos **9** (1999) 183–194.

[45] J. L. Thiffeault, Advection–diffusion in Lagrangian coordinates, Phys. Lett. A **309** (2003) 415–422.

[46] J. E. Truscott and J. Brindley, Ocean plankton populations as excitable media, Bull. Math. Biol. **56** (1994) 981–998.

[47] J. E. Truscott and J. Brindley, Equilibria, stability and excitability in a general class of plankton population models, Philos. Trans. R. Soc. London, Ser. A **347** (1994) 703–718.

[48] M.Vinson, Interactions of spiral waves in inhomogeneous excitable media, Physica D **116** (1998) 313–324.

[49] V. S. Zykov, *Simulation of Wave Processes in Excitable Media*, Manchester University Press, New York, 1987.